

Power flow analysis for a floating sandwich raft isolation system using a higher-order theory

W.J. Choi*, Y.P. Xiong, R.A. Shenoi

School of Engineering Sciences, Ship Science, University of Southampton, Highfield, Southampton SO17 1BJ, UK

Received 22 January 2008; received in revised form 13 May 2008; accepted 13 May 2008

Handling Editor: C.L. Morfey

Available online 24 June 2008

Abstract

A higher-order sandwich theory is implemented in conjunction with an equivalent mobility-based power flow progressive method to determine power flow for a sandwich configured floating raft vibration isolation system. The power spectrum changes in whole frequency range effectively when core materials' properties change. It is also shown that the loss factors of the sandwich configured floating raft influence the power flow transmitted to the foundation effectively in the medium- to high-frequency range and that the resonant peak cannot be avoided by increasing damping only in high-frequency ranges which is not found in floating raft isolation systems with isotropic beams.

© 2008 Elsevier Ltd. All rights reserved.

1. Introduction

Power flow analysis (PFA) approaches have been used to predict dynamic characteristics of coupled systems composed of various subsystems. The fundamental concept of power flow is discussed by Goyder and White [1] and Pinnington and White [2]. In recent years, this approach has been developed and applied to model complex structure [3–12] and to assess passive, active and vibration control system [8,13–17]. Langley [3] presented the dynamic stiffness method to investigate forced vibration of a row of stiffened rectangular panels, simply supported along the longitudinal edges. Clarkson [4] applied the receptance method to investigate the transmission of vibrational energy across structural joints of connected beams and connected plates. Cuschieri [5] used a mobility method to analyse the power flow in periodically connected beams and L-plates subject to a single excitation. Hussein and Hunt [6] applied the mean power flow method to evaluate the effectiveness of vibration countermeasures of an underground tunnel model which consisted of Euler–Bernoulli beams to account for the rails and the track slab. For complex structures, finite element analysis (FEA) is often used to analyse dynamic behaviours with good accuracy in low-frequency range. Jenkins et al. [7] used a finite element model to demonstrate the detailed dynamics of a typical raft-isolation-receiver system using secondary force inputs in parallel with a passive isolation system. They showed that a combined active/passive isolation system is more effective than a passive isolation system at low frequencies. Qu and Selvam [18] developed dynamic

*Corresponding author.

E-mail address: wjc@soton.ac.uk (W.J. Choi).

condensation to reduce the number of degrees of freedom (DOF) of finite element models for a damped system. However FEA schemes are usually computationally expensive because of relatively large number of DOF needed to capture the shorter wavelengths of vibration. Thus, it is difficult to analyse problem with high-frequency ranges.

The frequency response function method is more suitable to a system consisting of only two subsystems. However as the number of subsystems increases so the computational effort increases. The four-pole parameters method [19,20] is a classical technique for deriving dynamic characteristics of an assembled system connected in series or in parallel. This is convenient when considering a series of dynamical elements connected end-to-end. However, it is limited to single-input/single-output (SISO) linear mechanical systems. The four-pole parameters method was extended to multiple-input/multiple-output (MIMO) linear systems considering coupling interactions by Ha and Kim [21] to predict the frequency response characteristics and by Xiong [8] to estimate power flow transmission mechanisms.

PFA has become widely used to predict vibrational power flows through various kinds of assembled structures. Xiong et al. [9] investigated power flow in a flexible floating raft isolation system using the substructure mobility synthesis method. For a generic coupled system consisting of any number of substructures, Xiong et al. [10] developed progressive approaches to PFA and applied them to a complex coupled floating raft vibration isolation system. Generalized mobility/impedance matrix formulations of each substructure were derived allowing the construction of equivalent mobility and equivalent impedance matrices to describe the dynamic behaviour of a substructure assembled from several inter-connected substructures within the overall system. Application examples showed that an increase in dynamic stiffness of the raft reduces the vibrating power transmitted from the machinery via the raft to the flexible foundation.

A sandwich type floating raft system offers the advantage that the whole system is much lighter in addition to reducing vibration and noise [22]. Sandwich configurations are used where high stiffness/weight and strength/weight ratios are required. The flexural stiffness of a sandwich beam is proportional to $d^2h/4$, where d and h are the thickness of the core material and skin, respectively. Due to the high stiffness/weight which results in a higher natural frequency, the number of responding modes is drastically reduced [23]. Another advantage of using a sandwich configuration is that power flow levels tend to reduce as the viscoelasticity level of the core material increases [11]. Investigation on an active vibration control of energy flow from a machine transmitted to equipment, both mounted on a simply supported PVC sandwich panel, showed that increasing damping ratio of the core material of the sandwich panel reduces the resonant peaks of power flow transmission spectra to the equipment [11]. Sandwich structures with viscoelastic cores such as PVC that have relatively high ratios of energy dissipation to energy storage capability have been used in a variety of structural engineering applications where damping is required to dissipate energy [24].

Analytical models for sandwich structures have been studied using classical sandwich theory [25], first shear deformation theory [26], elastic foundation model [27] and various higher-order models where the higher-order terms are defined at the neutral axis [28]. However, these models have a drawback when sandwich structures are thick, the ratio of the transverse shear modulus to in-plane is low, and the ratio of longitudinal to transverse Young's moduli is high [29]. The characterization of sandwich structure with soft cores need to be simulated with the aid of an enhanced theory that can constitute its vertical flexibility which affects stress and displacement fields in the face sheets and influences nonlinear displacement patterns along the height of the core [30]. Most recently developed higher-order sandwich panel theory (HSAPT) [31] has shown the accuracy of predicted stress, localized effect and eigenvalue problems and validated by experimental results [30,32].

Gupta and Nakra [22] investigated effective vibration isolation by the use of an excitation system supported flexibly on a three-layer sandwich beam. However, this was analysed separately as a continuous system by a lumped mass supported on a spring and dash-pot. Li et al. [12] studied power flow via a floating raft consisting of a three-layer sandwich beam connected to two sandwich foundation beams of the same type. However, higher-order effects owing to the nonlinear displacement pattern of the core material were not considered. Since the flexibility affects internal resultants in skins, peeling and shear stresses in the core [25,33], the transverse shear interaction between skins and core material is also an important factor in the vibration response of a sandwich beam with a soft core, which induces the damping for sandwich structure with viscoelastic cores [29].

In this paper, the HSAPT is implemented in conjunction with progressive approaches of PFA to determine power flows in a sandwich configured floating raft vibration isolation system.

2. Application of power flow progressive method

The equivalent mobility-based power flow progressive approach [10] is applied. The general coupled system consisting of each substructure $S_1, S_2, \dots, S_i, \dots, S_n$ is shown in Fig. 1. The power flow transmitted into any substructure is given by

$$P_i = \frac{1}{2} \text{Re}\{\mathbf{F}_i^H \cdot \mathbf{v}_i\}, \quad i = 1, 2, \dots, n, \tag{1}$$

where P_i denotes the power flow through any interface of the i th substructure, H the Hermitian transpose, the force vectors and velocity response vectors are determined by the following progressive formulations [10]:

$$\begin{aligned} \mathbf{v}_i &= \mathbf{A}_i^e \cdot \mathbf{F}_i + \mathbf{N}_i^v \cdot \hat{\mathbf{v}}_{n+1}, \\ \mathbf{F}_{i+1} &= [\mathbf{A}_{i+1}^e - \mathbf{A}_i^{22}]^{-1} \cdot \mathbf{A}_i^{21} \cdot \mathbf{F}_i + [\mathbf{A}_i^{22} - \mathbf{A}_{i+1}^e]^{-1} \cdot \mathbf{N}_{i+1}^v \cdot \hat{\mathbf{v}}_{n+1}, \\ \mathbf{A}_i^e &= \mathbf{A}_i^{11} - \mathbf{A}_i^{12} \cdot [\mathbf{A}_i^{22} - \mathbf{A}_{i+1}^e]^{-1} \cdot \mathbf{A}_i^{21}, \\ \mathbf{N}_i^v &= \mathbf{A}_i^v \cdot \mathbf{A}_{i+1}^v \dots \mathbf{A}_n^v, \\ \mathbf{A}_i^v &= \mathbf{A}_i^{12} \cdot [\mathbf{A}_i^{22} - \mathbf{A}_{i+1}^e]^{-1} \quad (i = 1, 2, \dots, n), \\ \mathbf{A}_{n+1}^e &= \mathbf{0}, \end{aligned} \tag{2}$$

where \mathbf{A}_i^e is the equivalent mobility matrix of substructure S_i coupled to subsystems S_{i+1}, \dots, S_n ($i = 1, 2, \dots, n$) and \mathbf{N}_i^v is the velocity transmissibility matrix which represents the velocity response vector \mathbf{v}_i produced by a unit velocity input $\hat{\mathbf{v}}_{n+1}$, and it reflects the effect of the boundary motion excitations $\hat{\mathbf{v}}_{n+1}$ upon substructure S_i ($i = 1, 2, \dots, n$).

A floating sandwich raft isolation system as shown in Fig. 2 comprises: (1) rigid masses representing the source of vibration such as machinery, e.g. substructure S_1 ; (2) viscoelastic isolators, e.g. substructure S_2 and S_4 ; (3) a sandwich floating raft, e.g. substructure S_3 ; and (4) a sandwich beam base structure, e.g. substructure S_5 .

For substructure S_1 , with two inputs and four outputs of the two rigid masses, it is assumed that each mass is supported by two isolators which behave in a passive way, and that motion takes place only in the vertical direction. The generalized mobility matrix \mathbf{A}_1 is as follows:

$$\begin{Bmatrix} \mathbf{v}_1 \\ \mathbf{v}_2 \end{Bmatrix} = \begin{bmatrix} \mathbf{A}_1^{11} & \mathbf{A}_1^{12} \\ \mathbf{A}_1^{21} & \mathbf{A}_1^{22} \end{bmatrix} \cdot \begin{Bmatrix} \mathbf{F}_1 \\ \mathbf{F}_2 \end{Bmatrix}, \tag{3}$$

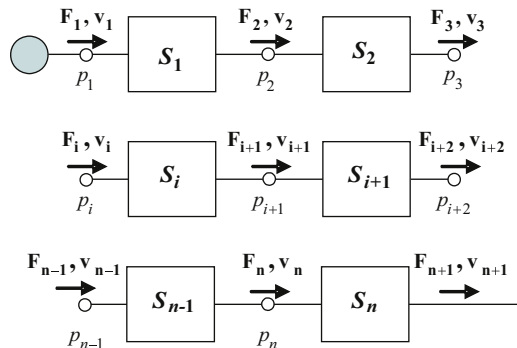


Fig. 1. Schematic illustration of the coupled systems with n substructures.

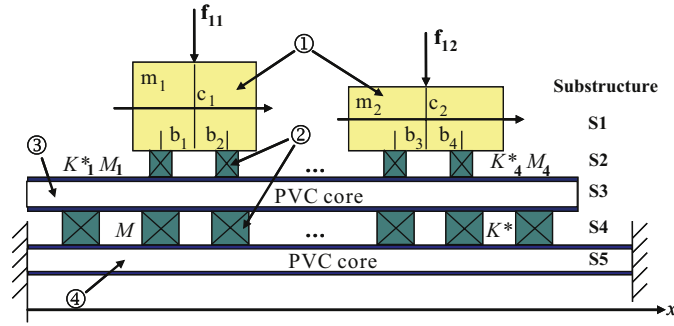


Fig. 2. Floating sandwich raft vibration isolation system (1. rigid mass, 2. isolators, 3. sandwich floating raft, 4. sandwich base structure).

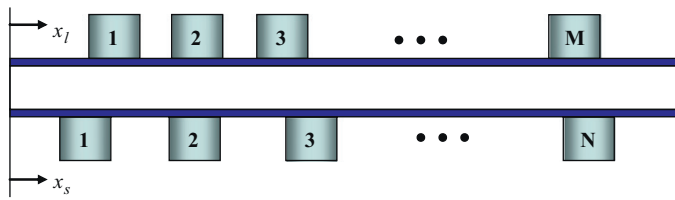


Fig. 3. Schematic figure to express mobility matrix and normal mode functions at each skin of sandwich beam.

where \mathbf{F}_1 is the prescribed excitation force and the sub-matrices of matrix \mathbf{A}_1 are given by

$$\mathbf{A}_1^{11} = \frac{1}{j\omega} \begin{bmatrix} 1/m_1 & 0 \\ 0 & 1/m_2 \end{bmatrix}, \tag{4}$$

$$\mathbf{A}_1^{12} = \frac{1}{j\omega} \begin{bmatrix} 1/m_1 & 1/m_1 & 0 & 0 \\ 0 & 0 & 1/m_2 & 1/m_2 \end{bmatrix}, \quad \mathbf{A}_1^{21} = [\mathbf{A}_1^{12}]^T, \tag{5}$$

$$\mathbf{A}_1^{22} = \frac{1}{j\omega} \begin{bmatrix} \begin{bmatrix} \frac{1}{m_1} + \frac{b_1^2}{J_1} & \frac{1}{m_1} - \frac{b_1 b_2}{J_1} \\ \frac{1}{m_1} - \frac{b_1 b_2}{J_1} & \frac{1}{m_1} + \frac{b_1^2}{J_1} \end{bmatrix} & \mathbf{0}_{2 \times 2} \\ \mathbf{0}_{2 \times 2} & \begin{bmatrix} \frac{1}{m_2} + \frac{b_3^2}{J_2} & \frac{1}{m_2} - \frac{b_3 b_4}{J_2} \\ \frac{1}{m_2} - \frac{b_3 b_4}{J_2} & \frac{1}{m_2} + \frac{b_3^2}{J_2} \end{bmatrix} \end{bmatrix}. \tag{6}$$

Fig. 3 shows the sandwich beam (S_3) which is the floating raft as shown in Fig. 2. For the isolator substructure S_2 consisting of M identical isolators, the generalized mobility matrix \mathbf{A}_2 is presented by

$$\mathbf{A}_2^{11} = \text{diag} \left[\frac{1}{j\omega M_l} + \frac{j\omega}{2K_l^*} \right]_{M \times M}, \tag{7}$$

$$\mathbf{A}_2^{12} = \text{diag} \left[\frac{1}{j\omega M_l} \right]_{M \times M} = \mathbf{A}_2^{21}, \tag{8}$$

$$\mathbf{A}_2^{22} = \mathbf{A}_2^{11}, \tag{9}$$

where M_l is the mass of each isolator. Similarly, for the isolator substructure S_4 consisting of N identical isolators shown in Fig. 3, the generalized mobility matrix \mathbf{A}_4 is presented by

$$\mathbf{A}_4^{11} = \text{diag} \left[\frac{1}{j\omega M_s} + \frac{j\omega}{2K_s^*} \right]_{N \times N}, \quad (10)$$

$$\mathbf{A}_4^{12} = \text{diag} \left[\frac{1}{j\omega M_s} \right]_{N \times N} = \mathbf{A}_4^{21}, \quad (11)$$

$$\mathbf{A}_4^{22} = \mathbf{A}_4^{11}, \quad (12)$$

where M_s is the mass of each isolator. For the flexible raft structure S_3 , the mobility matrix \mathbf{A}_3 can be derived by using a modal analysis method as follows:

$$\mathbf{A}_3^{11} = [\chi_{ls}(x_l^{(3)}, x_s^{(3)})]_{M \times M}, \quad (13)$$

$$\mathbf{A}_3^{12} = [\chi_{ls}(x_l^{(3)}, x_s^{(4)})]_{M \times N}, \quad (14)$$

$$\mathbf{A}_3^{21} = [\chi_{ls}(x_l^{(4)}, x_s^{(3)})]_{N \times M}, \quad (15)$$

$$\mathbf{A}_3^{22} = [\chi_{ls}(x_l^{(4)}, x_s^{(4)})]_{N \times N}, \quad (16)$$

where $x_l (l = 1, 2, 3, \dots, M)$ are the positional co-ordinates of the isolators in the substructure S_2 mounted between the rigid masses and the top skin of the sandwich floating raft in the substructure S_3 , and $x_s (s = 1, 2, 3, \dots, N)$ denote the positional coordinates of the substructure S_4 mounted between the sandwich floating raft and the sandwich base structure. Here, the components of the mobility matrix \mathbf{A}_3^{12} of the floating raft can be described as follows:

$$\chi_{ls}(x_l^{(3)}, x_s^{(4)}) = \frac{j\omega}{m} \sum_{n=1}^{\infty} \frac{\psi_n^{(3)}(x_l^{(3)})\psi_n^{(4)}(x_s^{(4)})}{[\Omega_n^{(3)}]^2(1 + j\eta_n^{(3)}) - \omega^2} \quad (l = 1, \dots, M, s = 1, \dots, N), \quad (17)$$

where the normal mode functions of the top and bottom skins of the free sandwich beam for the raft structure in S_3 are denoted by $\psi_n^{(3)}$ and $\psi_n^{(4)}$, respectively.

Similarly, the mobility matrix of the base sandwich structure S_5 can be described as follows:

$$\mathbf{A}_5 = [\Xi_{sk}(x_s^{(5)}, x_k^{(5)})]_{N \times N} \quad (s, k = 1, 2, \dots, N). \quad (18)$$

The components of the mobility matrix of the base structure can be described as follows:

$$\Xi_{sk}(x_s^{(5)}, x_k^{(5)}) = \frac{j\omega}{m} \sum_{n=1}^{\infty} \frac{\varphi_n^{(5)}(x_s^{(5)})\varphi_n^{(5)}(x_k^{(5)})}{[\Omega_n^{(5)}]^2(1 + j\eta_n^{(5)}) - \omega^2}, \quad (19)$$

where $\varphi_n^{(5)}$ denotes the normal mode functions of the top skins of the clamped sandwich beam for the base structure in S_5 .

The analysis of normal mode function and loss factor for sandwich beams is described in Section 3.

3. Natural vibration characteristics of sandwich beams using higher-order theory

In order to estimate the total power flow in a sandwich floating raft isolation system, the natural characteristics of sandwich structures need to be studied first. For numerical simplicity the floating raft, substructure S_3 , can be modelled as a free–free sandwich beam while the base structure, substructure S_5 , can be modelled as a clamped–clamped sandwich beam.

To estimate the natural vibration characteristics of a sandwich beam, the homogeneous solution including natural frequencies and corresponding modes needs to be obtained. Then the variation of mode shapes and natural frequencies with free–free and clamped beam at both ends are deduced.

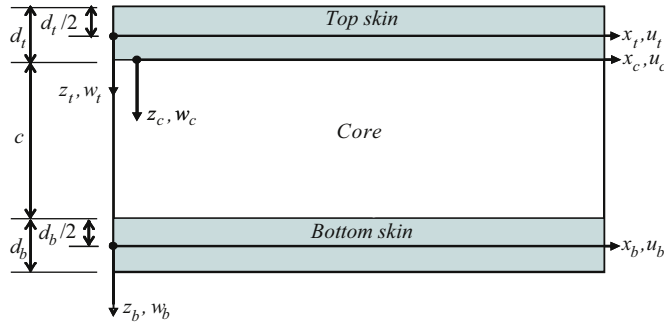


Fig. 4. Geometry of sandwich beam [36].

There are many possible approaches to predict vibration behaviour of a sandwich beam, including classical sandwich theory, elastic foundation models and various higher-order theories [34,35]. Since a shear-induced effect caused by the flexibility of the core needs to be modelled, a HSAPT appears to be most appropriate [34,36,37].

The geometry of a typical sandwich beam is illustrated in Fig. 4. In HSAPT, the skins of the sandwich beam are modelled as ordinary beams, without shear strains, that follow Euler–Bernolli assumptions and are subjected to small deformations. The transversely flexible core layer is considered as a two-dimensional elastic medium with small deformations where its thickness may change under loading, and its cross section does not remain planar. The longitudinal (in-plane) stresses in the core can be neglected owing to the low flexural stiffness of the core material. The interface layers between the skins and the core are assumed to be bonded perfectly and to provide continuity of the deformations at the interfaces. From variational calculus, the governing equations based on Frostig’s HSAPT are extended to include viscoelastic material properties in terms of each variation (δu_t , δu_b , δw_t , δw_b , $\delta \tau_c$) as in the following equations:

$$E^* A_t u_{t,xx} + b \tau_c - (m_t + m_c/3) \ddot{u}_t - (m_c/6) \ddot{u}_b + (m_c d_t/6) \ddot{w}_{t,x} - (m_c d_b/12) \ddot{w}_{b,x} = 0, \quad (20)$$

$$E^* A_b u_{b,xx} - b \tau_c - (m_b + m_c/3) \ddot{u}_b - (m_c/6) \ddot{u}_t - (m_c d_b/6) \ddot{w}_{b,x} + (m_c d_t/12) \ddot{w}_{t,x} = 0, \quad (21)$$

$$E^* I_t w_{t,xxxx} - ((c + d_t)b/2) \tau_{c,x} - (b E_c^*/c)(w_b - w_t) + (m_t + m_c/3) \ddot{w}_t + (m_c/6) \ddot{w}_b + (m_c d_t/6) \ddot{u}_{t,x} + (m_c d_t/12) \ddot{u}_{b,x} - (m_c d_t^2/12) \ddot{w}_{t,xx} + (m_c d_t d_b/24) \ddot{w}_{b,xx} = 0, \quad (22)$$

$$E^* I_b w_{b,xxxx} - ((c + d_b)b/2) \tau_{c,x} + (b E_c^*/c)(w_b - w_t) + (m_b + m_c/3) \ddot{w}_b + (m_c/6) \ddot{w}_t - (m_c d_b/6) \ddot{u}_{b,x} + (m_c d_b/12) \ddot{u}_{t,x} - (m_c d_b^2/12) \ddot{w}_{b,xx} + (m_c d_t d_b/24) \ddot{w}_{t,xx} = 0, \quad (23)$$

$$u_b - u_t - (c/G_c^*) \tau_c + ((c^3/12)/E_c^*) \tau_{c,xx} + ((c + d_t)/2) w_{t,x} + ((c + d_b)/2) w_{b,x} = 0, \quad (24)$$

where A_t , A_b are cross-sectional areas of the top and bottom skins and I_t , I_b are second moments of inertia of the top and bottom skins, respectively and E^* , E_c^* and G_c^* are the complex Young’s moduli of skins and core and the complex shear modulus of the core, respectively, and

$$E^* = E' + iE'', \quad (25)$$

$$E_c^* = E'_c + iE''_c, \quad (26)$$

$$G_c^* = G'_c + iG''_c, \quad (27)$$

where E' , E'_c , G'_c are the storage moduli and E'' , E''_c , G''_c are the loss moduli of the phase properties.

The boundary conditions for the top and bottom skins at the left ($x = 0$) and right ($x = L$) edges of the sandwich beam are as follows:

$$N_{xx}^p(x = 0, L) = E^* A_p u_{p,x} = 0 \text{ or } u_p = 0, \quad (28)$$

$$M_{xx}^p(x = 0, L) = E^* I_p w_{p,xx} = 0 \text{ or } w_{p,x} = 0, \quad (29)$$

$$E^* I_t w_{t,xxx} - (d_t b/2)\tau_c + (m_c d_t/6)\ddot{u}_t + (m_c d_t/12)\ddot{u}_b - (m_c d_t^2/12)\ddot{w}_{t,x} + (m_c d_t d_b/24)\ddot{w}_{b,x} = 0, \quad (30)$$

$$E^* I_t w_{b,xxx} - (d_b b/2)\tau_c - (m_c d_b/12)\ddot{u}_t - (m_c d_b/6)\ddot{u}_b - (m_c d_b^2/12)\ddot{w}_{b,x} + (m_c d_t d_b/24)\ddot{w}_{t,x} = 0, \quad (31)$$

where N_{xx}^p and M_{xx}^p are the axial force and the bending moment capabilities of the skins.

The boundary conditions relevant to any point along the height (z) of the core are as follows:

$$\tau_c(x = 0) = 0, \quad \tau_c(x = L) = 0 \quad \text{or}$$

$$w_c(x = 0, z = Z_c) = 0, \quad w_c(x = L, z = Z_c) = 0. \quad (32)$$

The general vibration equation of motion can be written as

$$[\mathbf{M}][\ddot{\mathbf{A}}] + [\mathbf{K}^*][\mathbf{A}] = 0, \quad (33)$$

where $[\mathbf{M}]$ is the mass matrix and $[\mathbf{K}^*]$ the complex stiffness matrix.

The displacement vector is

$$[\mathbf{A}]^T = [w_t \ w_b \ u_t \ u_b \ \tau_c], \quad (34)$$

where w_t , w_b and u_t , u_b are the displacements of top and bottom surfaces of the beam in the vertical and the horizontal directions, respectively.

To analyse free vibration, assuming harmonic behaviour in time, a general solution of the form, $[\mathbf{A}] = [\mathbf{A}] \exp(i\omega t)$ is considered where ω is the complex eigen frequency and t is the time. Thus governing Eq. (33) is changed

$$([\mathbf{K}^*] - \lambda^*[\mathbf{M}])[\mathbf{A}] = 0, \quad (35)$$

where λ^* is a complex eigenvalue, $[\mathbf{A}]$ is the matrix of eigenvectors and $[\mathbf{M}]$ and $[\mathbf{K}^*]$ are ordinary symmetric matrices of the mass and frequency-dependent complex stiffness, respectively, details of which are given in Appendix A. The full solution of the free vibration problem is achieved with the appropriate boundary conditions. After obtaining the complex eigenvalues, the complex circular frequency Ω^* and the modal loss factor η_n of the sandwich beam can be calculated for each mode from

$$\lambda_n^* = \lambda_n' + i\lambda_n'', \quad \eta_n = \frac{\lambda_n''}{\lambda_n'}, \quad (36)$$

where, λ_n' and λ_n'' are real and imaginary eigenvalues, respectively [38]. The transverse displacement of each skin $w_p(x, t)$, is

$$w_p(x, t) = \sum_{n=1}^{\infty} \psi_n^p(x) q_n^p(t), \quad (37)$$

where $\psi_n^p(x)$ are mass normalized mode shapes as described in Eqs. (17) and (19) and $q_n^p(t)$ is time-dependent coordinates, respectively, p denotes t (top) or b (bottom).

Numerical free vibration analyses results using this higher-order sandwich theory implementation are validated with FEA solutions in Appendix B.

4. Power flow analysis for sandwich floating raft vibration isolation system

For numerical calculations, the following data are used: $m_1 = 50$ kg, $m_2 = 30$ kg, $b_{ij} = 25$ mm ($i, j = 1, 2$). The stiffness and mass of the isolator in substructure 2 is 20 N/mm (K_I) and 0.5 kg (M_I) and those of the isolator in substructure 4 is 40 N/mm (K_S) and 0.5 kg (M_S). Four isolators, two at each mass, are used in

substructure 2 while three isolators are used in substructure 4. The loss factor (η_I) of the isolators in substructures 2 and 4 is 0.05. Vertical harmonic excitation forces are of the forms $f_{11} = e^{i\omega t}$, $f_{12} = 2f_{11}$. The sandwich beam in substructures S_3 and S_5 consists of two glass–ceramic skins of dimensions $300 \times 30 \times 1.0 \text{ mm}^3$ which are bonded to the top and bottom of a PVC core of dimensions $300 \times 30 \times 20 \text{ mm}^3$. Young's modulus of the isotropic glass–ceramic skins and the shear modulus of the core are 36 GPa and 20 MPa, respectively and the respective densities of the skins and core are 4,400 and 52.06 kg/m³, as used in Sokolinsky et al. [30]. The loss factor (η_I) of the core materials is 0.05.

4.1. Input power and transmitted power

Fig. 5 compares the input power spectrum P_1 owing to the two machines to the total power flow transmission spectra P_3 and P_5 . The difference between them indicates the energy dissipated in this raft isolation system. It can be seen that the input power flow spectrum P_1 is relatively simple in form with three pronounced peaks corresponding to the natural frequencies of the isolation system. The transmission spectra P_3 and P_5 , however, vary significantly with the exciting frequencies in the medium- and high-frequency range, since they now contain contributions from the elastic mode coupled dynamics of the overall system. The relatively small number of coupled system and intermediate mass of isolators at substructure 3 reduce the number of peaks and power spectrum P_3 , respectively. The number of peaks indicate that the total input power spectrum P_1 is less sensitive than the total transmitted power spectrum to the changes of the excitation frequencies as shown in Fig. 5. The behaviour of the power flow spectrum is supported by numerical results [10]. Based on the parameters described in the previous section, the influence of different variables such as thickness of core, thickness of skin, stiffness of sandwich raft and base structure and the effect of isolators on power transmitted to the flexible foundation are discussed below.

4.2. Effect of sandwich raft on power transmissions

Fig. 6 compares power flow spectra P_5 considering different thicknesses of core material in substructure 3. When the thickness of the core increases from 20 to 80 mm, the transmitted power spectrum decreases. The reason for this is that when the thickness of the core increases the stiffness of the sandwich beam also increases, which results in decreasing power transmitted to the base structure. This again is supported by the conclusion in Xiong et al. [39]. This indicates that an increase in core thickness of the sandwich raft increases its stiffness, thus reducing the power transmitted to the foundation at low-frequency ranges, and alters

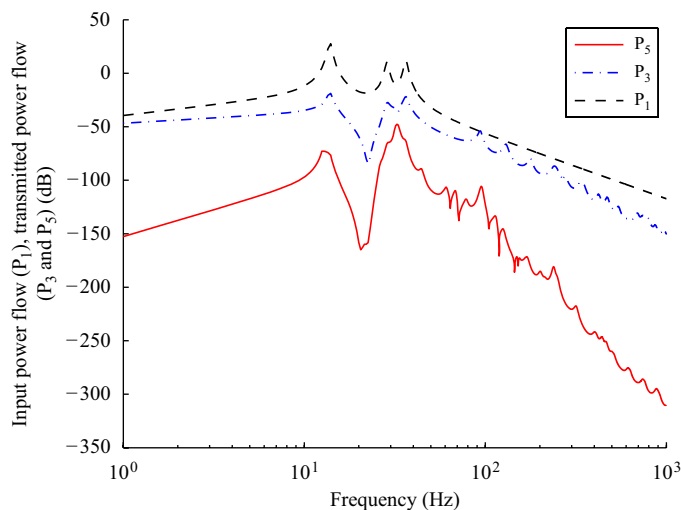


Fig. 5. Comparison of power flow spectra.

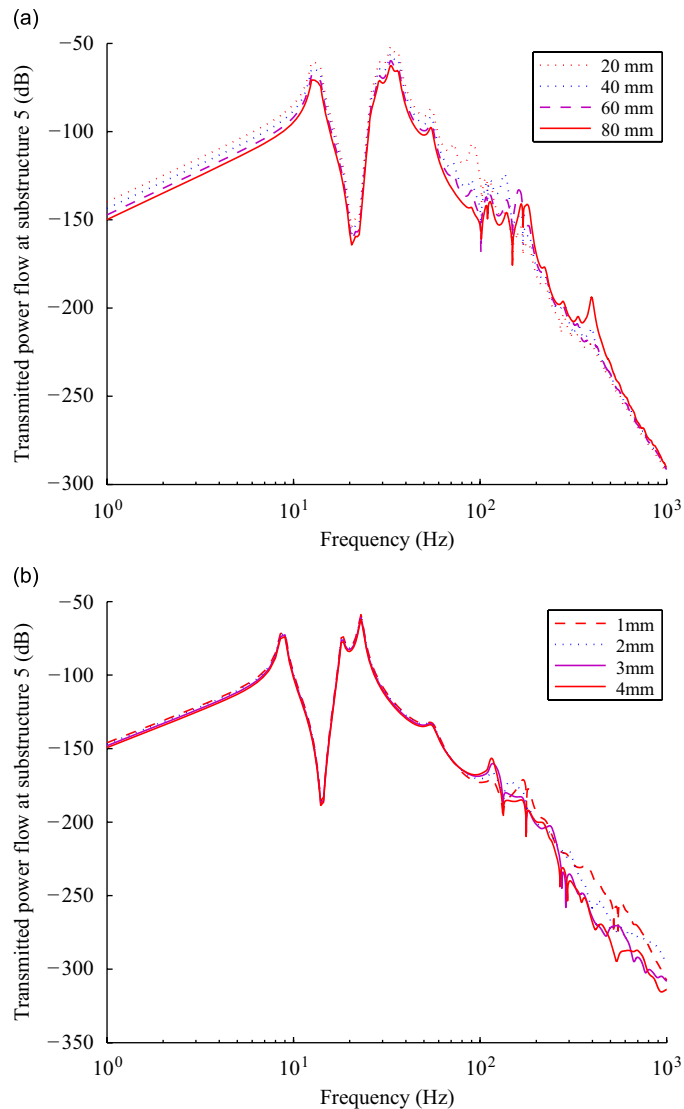


Fig. 6. Comparison of power flow spectra under the different thickness of (a) core material and (b) skin material in substructure 3.

resonant peaks at medium-frequency ranges, hence providing good vibration isolation. This result shows good agreement with the trends in Li et al. [12], i.e. that the transmitted energy decreases as thickness of the core increases. Fig. 6b compares power flow spectra with different thicknesses of skin material of the sandwich raft. The change in thickness of the skin materials does not affect the power spectrum at low-frequency ranges. From medium-frequency ranges to high-frequency ranges, the transmitted power spectrum decreases prominently with the increase of skin thickness.

4.3. Effect of sandwich base structure on power transmissions

Fig. 7a shows power flow spectra of the isolation system with different thickness of core material of sandwich beam in substructure 5. Similar to the result of Fig. 6a, the core thickness changes also affect the transmitted power. However, since decreased power flow from floating raft may not be effective to further decreasing power flow at foundation, change in the power flow spectrum of the foundation is less significant than that of the floating raft in the whole frequency range.

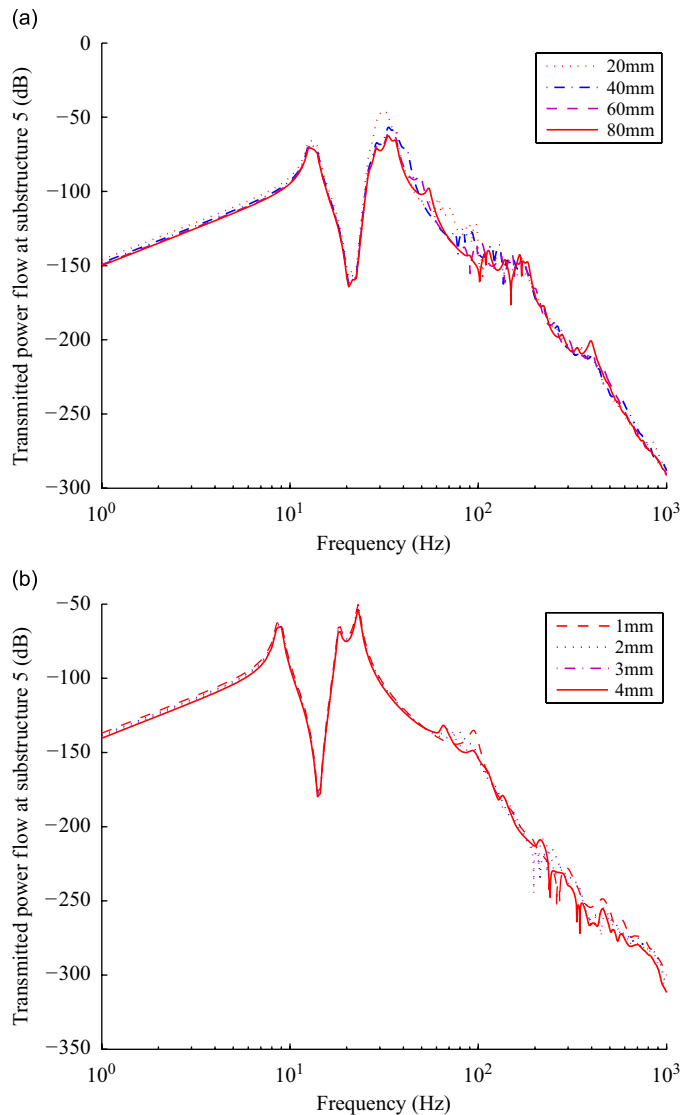


Fig. 7. Comparison of power flow spectra under the different thickness of (a) core material and (b) skin material in substructure 5.

Fig. 7b presents power flow spectra with different thicknesses of skin material of sandwich beam for substructure S_5 . The change in thickness of the skin material does not affect much on power spectrum in the whole frequency ranges. Even though there are power decreases at high frequencies, the power reduction is not much more effective than that of the floating raft, substructure S_3 .

4.4. Changing skin and core modulus of raft beam

Fig. 8a shows a comparison of power flow spectra with different properties of skin material of the sandwich beam in substructure 3. The reference Young's modulus (E_{ref}) of the skin material is 36 GPa. It is clear that even though the modulus changes by a ten-fold margin there is little effect on the power flow spectrum because it cannot reflect the whole stiffness of the floating raft effectively. Fig. 8b shows a comparison of power flow spectra with the different properties of core material of sandwich beam in substructure 3, where reference shear modulus (G_{ref}) of the core material is 20 MPa. This result shows that property change of the core material is more effective than that of the skin material.

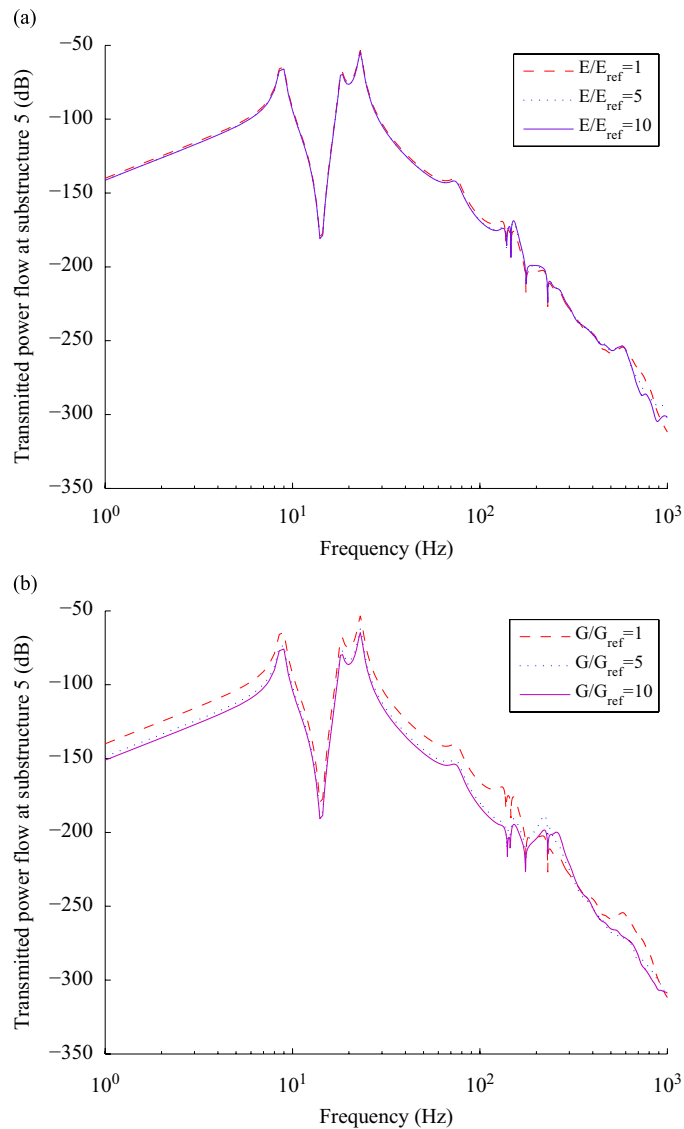


Fig. 8. Comparison of power flow spectra under the different properties of (a) skin material and (b) core material in substructure 3.

4.5. Effect of isolators

Fig. 9 shows a comparison of transmitted power spectra with different stiffness of the isolators in substructures 2 and 4. The respective reference stiffnesses (K_{ref}) of the isolators are 20 and 40 N/mm in substructures 2 and 4. Comparisons are made with isolators stiffnesses of one tenth and ten times that of the reference values, i.e. stiffness ratios of 0.1 and 10. Transmitted power spectrum changes as stiffness of the isolator changes. Contrary to the results of sandwich beam structure, transmitted power changes in inverse proportion to the change of the stiffness of the isolators. In Fig. 9a, the fundamental frequency of around 10 Hz is altered as the stiffness of the isolator changes. However after 20 Hz, the three curves of power spectrum are identical. Fig. 9b shows that in lower-frequency range the resonant peaks dominated by isolators are altered as the stiffness of the isolator changes up to 50 Hz. This is because the coupling effect of the two stage isolation system, in which the floating raft as well as base beam behave like rigid body. However above the frequency of 50 Hz the resonant peaks of the three power spectrum are identical because of the coupling effect of elastic modes of raft and base beams. Since the stiffness of the isolators in substructure 4 is higher

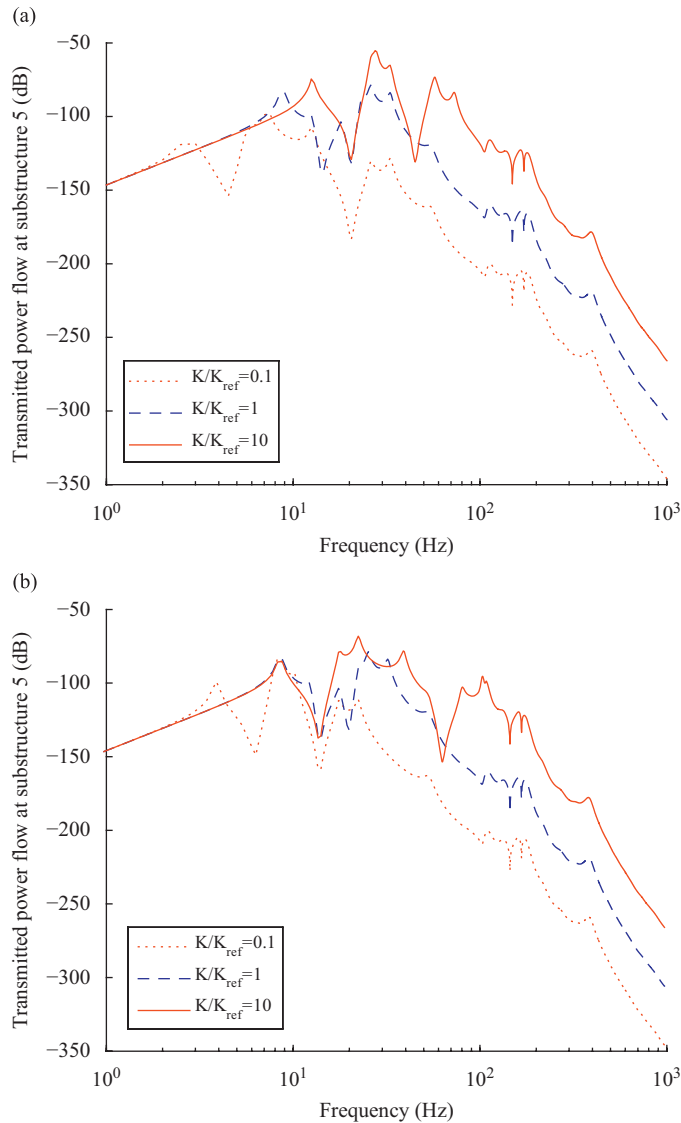


Fig. 9. Comparison of power flow spectra under the different stiffness of isolators between (a) substructure 2 and (b) substructure 4.

than that in substructure 2, the change of fundamental frequency ranges are shifted to higher-frequency ranges. These results show that coupling mechanism between isolators and flexible beams need to be considered in the design of the floating raft isolation systems.

4.6. Damping effect of core materials in sandwich raft beam

The influence of the damping effect for core materials of the floating raft can be observed in Fig. 10. It is shown that increasing the loss factor of the core material reduces the resonant peaks of the transmitted power flow spectra in the medium- to high-frequency ranges. At low-frequencies ranges, changes in the transmitted powers cannot be observed. Also, there is not much effect on the reduction of resonant peak prominently. However, the damping effect can be seen in the medium-frequency range at about 100 Hz. It is interesting to note that there is a pronounced peak observed in the transmitted power spectrum in P_5 at about 650 Hz. This is because the modal damping of the sandwich raft beam corresponding to the symmetric vibration mode of

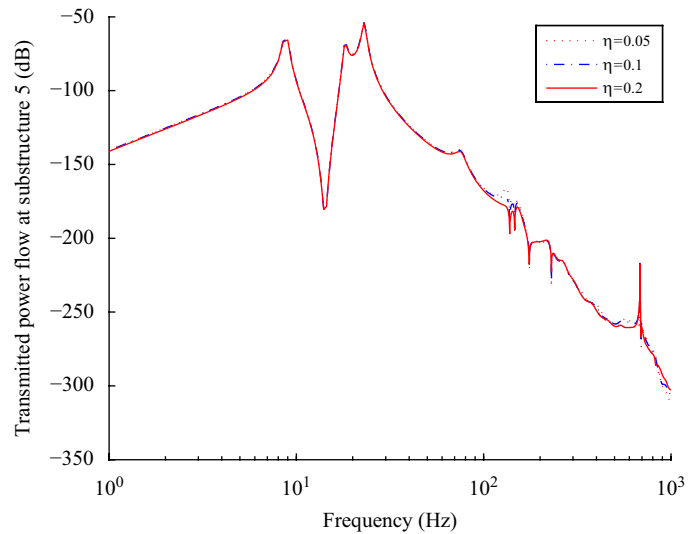


Fig. 10. Comparison of power flow spectra under the different damping of core material in substructure 3.

the beam is very small. This phenomenon can be explained from in Fig. 10 which shows different modal loss factors for each mode based on numerical calculation. This indicates that this resonant peak cannot be avoided by increasing damping only in the high-frequency ranges, which is not found in floating raft isolation system with isotropic beams. Further calculations show that this peak can be avoided by changing stiffness of the raft and placement of isolators.

5. Conclusion

A higher-order sandwich theory is implemented in conjunction with an equivalent mobility-based power flow progressive method to determine power flow for a sandwich configured floating raft vibration isolation system. The generalized mobility matrices of a sandwich floating raft and flexible foundation are derived using higher-order sandwich theory.

The results from the application of the models developed herein show the following attributes: (a) increasing thickness of the core material of sandwich type floating raft decreases transmitted power more effectively than that of foundation; (b) when different properties of core material of floating raft are used, the power spectrum varies in whole frequency range, which leads to the conclusion that when a sandwich beam is considered as a floating raft, the core material choice is more influential than that of skin material; (c) the stiffness change of isolators does not affect the pattern of power spectrum in medium- and high-frequency ranges, though compromises between numbers and stiffnesses of the isolators must be considered carefully; (d) the loss factors of a sandwich configured floating raft influence the power flow transmitted to the foundation effectively from medium- to high-frequency range. However the resonant peak corresponding to the symmetric mode of the sandwich raft in high-frequency ranges cannot be avoided by increasing damping only. The resonant peak can be avoided by changing stiffness of the raft and placement of isolators.

Acknowledgment

Y.P. Xiong and R.A. Shenoi wish to acknowledge support from MARSTRUCT, the EU-funded Network of Excellence in Marine Structures.

Appendix A. Component of mass and stiffness matrix for simply supported sandwich beam

From Eq. (35) matrices of the mass and the complex stiffness are presented as follows [38]:

$$[M] = \begin{bmatrix} m_t + \frac{1}{12}m_c d_t^2 \kappa^2 + \frac{1}{3}m_c & \frac{1}{6}m_c - \frac{1}{24}m_c d_t d_b \kappa^2 & -\frac{1}{6}m_c d_t \kappa & -\frac{1}{12}m_c d_t \kappa & 0 \\ \frac{1}{6}m_c - \frac{1}{24}m_c d_t d_b \kappa^2 & m_b - \frac{1}{12}m_c d_b^2 \kappa^2 + \frac{1}{3}m_c & \frac{1}{12}m_c d_b \kappa & \frac{1}{6}m_c d_b \kappa & 0 \\ \frac{1}{6}m_c d_t \kappa & -\frac{1}{12}m_c d_b \kappa & -m_t - \frac{1}{3}m_c & -\frac{1}{6}m_c & 0 \\ \frac{1}{12}m_c d_t \kappa & -\frac{1}{6}m_c d_b \kappa & -\frac{1}{6}m_c & -m_b - \frac{1}{3}m_c & 0 \\ 0 & 0 & 0 & 0 & 0 \end{bmatrix},$$

$$[K] = \begin{bmatrix} EI_t \kappa^4 + bE_c^*/c & -bE_c^*/c & 0 & 0 & \frac{1}{2}\kappa b(c + d_t) \\ -bE_c^*/c & EI_b \kappa^4 + bE_c^*/c & 0 & 0 & \frac{1}{2}\kappa b(c + d_b) \\ 0 & 0 & -EA_t \kappa^2 & 0 & b \\ 0 & 0 & 0 & -EA_b \kappa^2 & -b \\ \frac{1}{2}\kappa b(c + d_t) & \frac{1}{2}\kappa b(c + d_b) & -b & -b & \frac{c}{G_c^*} + \frac{c^3 b}{12E_c^* \kappa^2} \end{bmatrix},$$

where m_t , m_b , m_c are mass of top, bottom and core, respectively and b is the width of the core and κ is $n\pi/L$, where L is the length of the beam.

Table 1
Properties of the sandwich beam with a soft core [30]

Constituent	Material	Young's modulus (GPa)	Shear modulus (GPa)	Poisson's ratio	Density (kg/m ³)
Skins	GRP	36	13.84	0.3	4400
Core	PVC	0.05	0.02	0.25	52.060

Table 2
Comparison of natural frequencies of a sandwich beam with different boundary conditions (frequency, Hz)

Mode	Clamped		Free-free	
	ABAQUS	HSAPT	ABAQUS	HSAPT
1	419	419	697	670
2	835	842	1193	1169
3	1299	1316	1707	1685
4	1757	1786	2161	2148
5	2211	2256	2640	2637
6	2658	2724	3069	3086
7	3100	3191	3531	3572
8	3535	3659	3922	3994
9	3963	4126	4386	4306
10	4384	4306	4533	4503

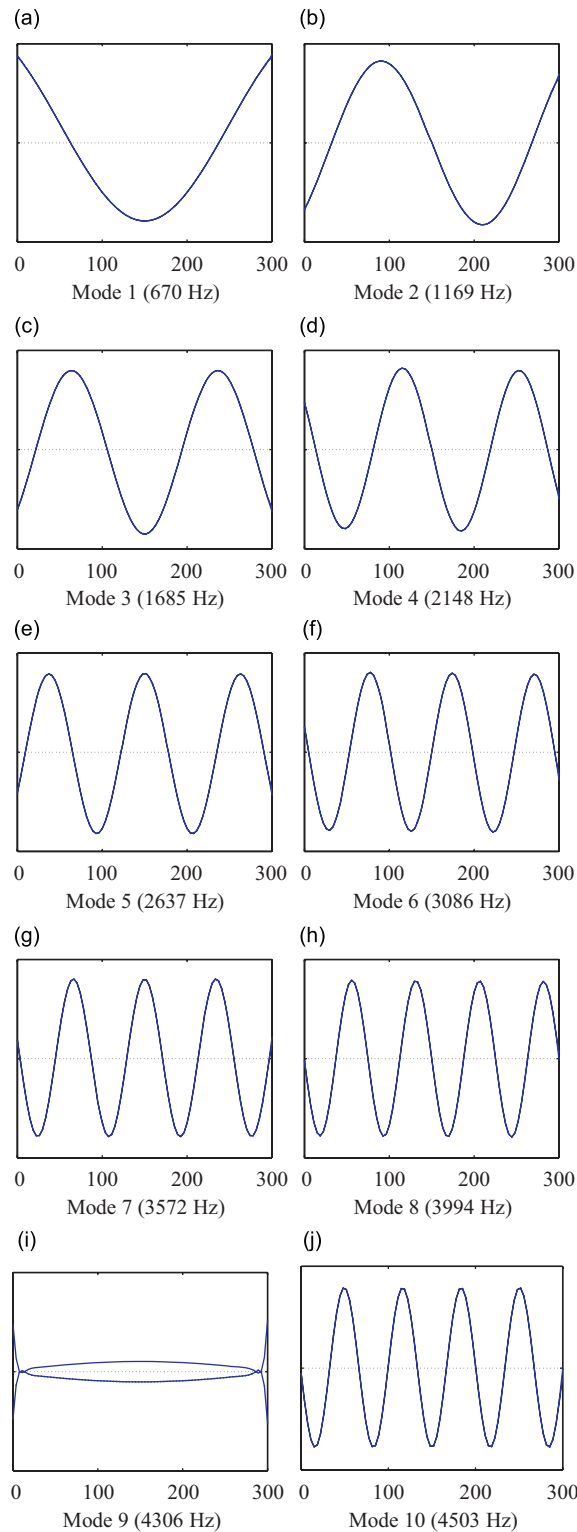


Fig. 11. Bending mode shape of the free beam at top skin (solid line) and bottom skin (dotted line) (abscissa—beam span in mm and ordinate—normalized displacement).

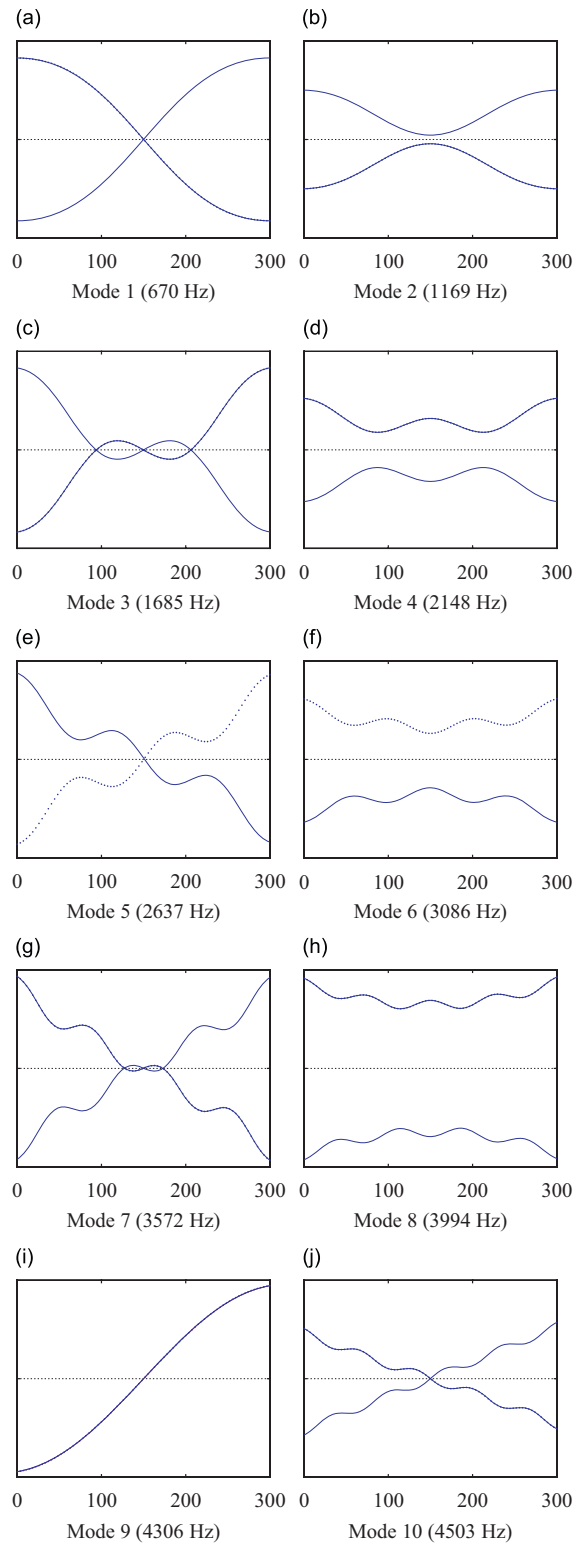


Fig. 12. Bending mode shape of the free beam at top skin (solid line) and bottom skin (dotted line) in axial mode (abscissa—beam span in mm and ordinate—normalized displacement).

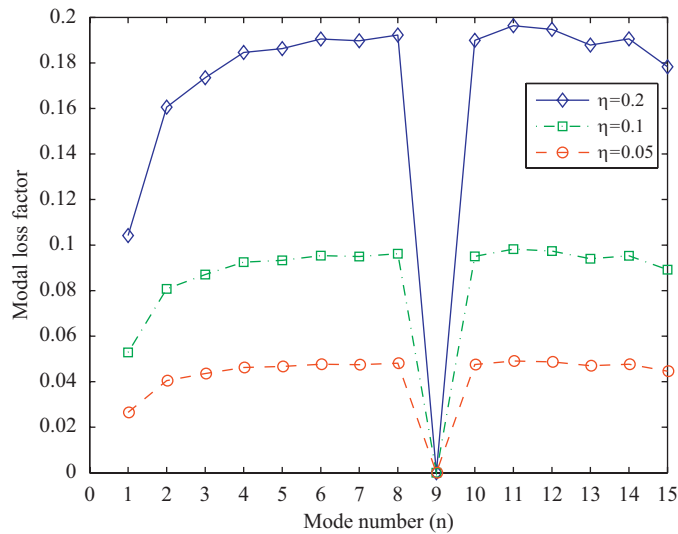


Fig. 13. Comparison of modal loss factors.

Appendix B. Validation of free vibration of sandwich beams

In order to estimate the total power flow in sandwich floating raft isolation systems, the natural characteristics of sandwich structures is of ultimate importance. In the vibration isolation system, free–free sandwich beam is regarded as a floating raft while clamped–clamped sandwich beam is considered as a base structure. Using higher-order sandwich plate theory, numerical free vibration analyses results are compared with FEA solutions. Based on these results, power flow analysis for a sandwich floating raft vibration isolation system can be presented.

The length of the beam is 300 mm, the width of the beam is 20 mm, the identical skins are 0.5 mm thick, and the thickness of the soft plastic foam core is 19.05 mm. The mechanical properties of the skins corresponding to an isotropic glass–ceramic material and those of the core corresponding to isotropic polymethacrylimide rigid foam are given in Table 1.

Natural frequencies of the sandwich beam for each boundary condition are presented in Table 2. The FEA model consists of 1800 elements and 1963 nodes using four bilinear node plain-strain quadrilateral elements (CPE4). The core has 10 layers of elements through the thickness while each skin has one layer of element through the thickness. The first 10 eigenvalues were obtained by using Lanczos eigenvalue solver (ABAQUS, 2006). Numerical results from Frostig’s higher-order sandwich theory matches well with those of FEA solutions.

Fig. 11 presents the bending mode shapes of the free–free sandwich beams, which change depending on the dimension and properties of skins and core materials. Most of vibration modes are similar to those of a homogeneous beam. The top and bottom skins move in phase with each other in the antisymmetric mode. However, the symmetric mode occurs at mode 9 as the skins move 180° out of phase with respect to beam’s neutral line. Both top and bottom skins are split at each edge with much smaller displacements [30].

Bending mode shapes in axial mode of the free–free sandwich beams are presented in Fig. 12. The results show that vibration mode shapes of top and bottom skins are symmetric except for mode 9. This indicates that antisymmetric behaviour in the bending mode corresponds to symmetric behaviour in the axial mode. Compressive and tensile forces at each skin contribute to the modal loss factor. Fig. 13 shows different modal loss factors for each mode based on numerical calculation. Note that the modal loss factor at mode 9 is nearly zero. This is because when both top and bottom skins move together in the same axial mode, there is no energy dissipation at the interface between the skins and core material.

References

- [1] H.G.D. Goyder, R.G. White, Vibration power flow from machines into built-up structures, *Journal of Sound and Vibration* 68 (1980) 59–117.
- [2] R.J. Pinnington, R.G. White, Power flow through machine isolators to resonant and non-resonant beam, *Journal of Sound and Vibration* 75 (1981) 179–197.
- [3] R.S. Langley, Analysis of power flow in beams and frameworks using the direct-dynamic stiffness method, *Journal of Sound and Vibration* 136 (3) (1990) 439–452.
- [4] B.L. Clarkson, Estimation of the coupling loss factor of structural joints, *Proceedings of the Institution of Mechanical Engineers Part C- Journal of Mechanical Engineering Science* 205 (1) (1991) 17–22.
- [5] J.M. Cuschieri, Vibration transmission through periodic structures using a mobility power flow approach, *Journal of Sound and Vibration* 143 (1) (1990) 65–74.
- [6] M.F.M. Hussein, H.E.M. Hunt, A power flow method for evaluating vibration from underground railways, *Journal of Sound and Vibration* 293 (3–5) (2006) 667–679.
- [7] M.D. Jenkins, P.A. Nelson, R.J. Pinnington, S.J. Elliott, Active isolation of periodic machinery vibrations, *Journal of Sound and Vibration* 166 (1) (1993) 117–140.
- [8] Y.P. Xiong, Power Flow Transmission Mechanism and Optimum Control of Complex Coupled Flexible System of Machinery and Foundation, PhD thesis, Shandong University of Technology, 1996.
- [9] Y.P. Xiong, K.J. Song, Power flow analysis for a new isolation system-flexible floating raft, *Chinese Journal of Mechanical Engineering* 9 (1996) 260–264.
- [10] Y.P. Xiong, J.T. Xing, W.G. Price, Power flow analysis of complex coupled systems by progressive approaches, *Journal of Sound and Vibration* 239 (2) (2001) 275–295.
- [11] Y.P. Xiong, J.T. Xing, W.G. Price, R.A. Sheno, Active control of energy flow from source to equipment on a sandwich panel, *Proceedings of the Fifth International Conference on Vibration Engineering*, Nanjing, China, China Aviation Industry, 2002.
- [12] T.Y. Li, X.M. Zhang, Y.T. Zuo, M.B. Xu, Structural power flow analysis for a floating raft isolation system consisting of constrained damped beams, *Journal of Sound and Vibration* 202 (1) (1997) 47–54.
- [13] D.W. Miller, S.R. Hall, A.H. von Flotow, Optimal control of power flow at structural junctions, *Journal of Sound and Vibration* 140 (1990) 475–497.
- [14] J. Pan, J. Pan, C.H. Hansen, Total power flow from a vibrating rigid body to a thin panel through multiple elastic mounts, *The Journal of the Acoustical Society of America* 92 (2) (1992) 895–907.
- [15] Y.P. Xiong, J.T. Xing, W.G. Price, Hybrid active and passive control of vibratory power flow in flexible isolation system, *Shock And Vibration* 7 (3) (2000) 139–148.
- [16] Y.P. Xiong, J.T. Xing, W.G. Price, A general linear mathematical model of power flow analysis and control for integrated structure–control systems, *Journal of Sound and Vibration* 267 (2) (2003) 301–334.
- [17] Y.P. Xiong, J.T. Xing, W.G. Price, A power flow mode theory based on a system's damping distribution and power flow design approaches, *Proceedings of the Royal Society A* 461 (2005) 3381–3411.
- [18] Z.Q. Qu, R.P. Selvam, Efficient method for dynamic condensation of nonclassically damped vibration systems, *AIAA Journal* 40 (2) (2002) 368–375.
- [19] C.T. Molly, Use of four-pole parameters in vibration calculations, *Journal of the Acoustical Society of America* 29 (1957) 842–853.
- [20] J.C. Snowdon, Mechanical four-pole parameters and their applications, *Journal of Sound and Vibration* 15 (1971) 307–323.
- [21] J.Y. Ha, K.J. Kim, Analysis of mimo mechanical systems using the vectorial four pole parameter method, *Journal of Sound and Vibration* 180 (2) (1995) 333–350.
- [22] R.C. Das Vikal, K.N. Gupta, B.C. Nakra, Vibration of an excitation system supported flexibly on a viscoelastic sandwich beam at its mid-point, *Journal of Sound and Vibration* 75 (1) (1981) 87–99.
- [23] D.J. Mead, *Passive Vibration Control*, Wiley, New York, 2000.
- [24] M. Meunier, R.A. Sheno, Dynamic analysis of composite sandwich plates with damping modelled using higher order theory, *Composite Structures* 54 (2001) 243–254.
- [25] H.G. Allen, *Analysis and Design of Structural Sandwich Panels*, Pergamon Press, Oxford, 1969.
- [26] J.M. Whitney, N.J. Pagano, Shear deformation in heterogeneous anisotropic plates, *Journal of Applied Mechanics* (1970) 1031–1036.
- [27] D. Zenkert, *An Introduction to Sandwich Construction*, The Chameleon Press Ltd, London, 1997.
- [28] J.N. Reddy, *Theory and Analysis of Laminated Composite Plates*, *Mechanics of Composite Materials and Structures*, 1999.
- [29] H. Hu, S. Belouettar, M. Potier-Ferry, E.M. Daya, Review and assessment of various theories for modeling sandwich composites, *Composite Structures* 84 (3) (2008) 282–292.
- [30] V.S. Sokolinsky, S.R. Nutt, Y. Frostig, Boundary condition effects in free vibration of higher-order soft sandwich beams, *American Institute of Aeronautics and Astronautics* 40 (2002) 1220–1227.
- [31] Y. Frostig, M. Baruch, I. Sheinman, High-order theory for sandwich beam behavior with transversely flexible core, *Journal of Engineering Mechanics* 118 (5) (1992) 1026–1043.
- [32] V.S. Sokolinsky, H.F. Bremen, J.A. Lavoie, S.R. Nutt, Analytical and experimental study of free vibration response of soft-core sandwich beams, *Journal of Sandwich Structures and Materials* 6 (2004) 239–261.
- [33] F.J. Plantema, *Sandwich Construction*, Wiley, New York, 1966.

- [34] Y. Frostig, M. Baruch, Free vibrations of sandwich beams with a transversely flexible core: a high order approach, *Journal of Sound and Vibration* 176 (2) (1994) 195–208.
- [35] R.A. Shenoi, A. Groves, Y.D.S. Rajapakse, *Theory and Applications of Sandwich Structures*, University of Southampton Press, 2005.
- [36] Y. Frostig, Behavior of delaminated sandwich beam with transversely flexible core-high order theory, *Composite Structures* 38 (1992) 383–394.
- [37] A.K. Nayak, S.S.J. Moy, R.A. Shenoi, A higher order finite element theory for buckling and vibration analysis of initially stressed composite sandwich plates, *Journal of Sound and Vibration* 286 (4–5) (2005) 763–780.
- [38] W.J. Choi, Y.P. Xiong, R.A. Shenoi, Vibration characteristics of smart sandwich beams embedded with magnetorheological elastomer cores, *First International Conference on Marine Structures*, March 12–14, Glasgow, UK, 2007, pp. 421–428.
- [39] Y.P. Xiong, K.J. Song, X. Ai, Influence of flexible foundation on isolator wave effects, *Shock And Vibration* 3 (1) (1996) 61–67.